Hindawi Publishing Corporation
EURASIP Journal on Applied Signal Processing
Volume 2006, Article ID 47534, Pages 1–16
DOI 10.1155/ASP/2006/47534

Multiresolution Signal Processing Techniques for Ground Moving Target Detection Using Airborne Radar

Jameson S. Bergin and Paul M. Techau

Information Systems Laboratories, Inc., 8130 Boone Boulevard, Suite 500, Vienna, VA 22182, USA

Received 1 November 2004; Revised 15 April 2005; Accepted 25 April 2005

Synthetic aperture radar (SAR) exploits very high spatial resolution via temporal integration and ownship motion to reduce the background clutter power in a given resolution cell to allow detection of nonmoving targets. Ground moving target indicator (GMTI) radar, on the other hand, employs much lower-resolution processing but exploits relative differences in the space-time response between moving targets and clutter for detection. Therefore, SAR and GMTI represent two different temporal processing resolution scales which have typically been optimized and demonstrated independently to work well for detecting either stationary (in the case of SAR) or exo-clutter (in the case of GMTI) targets. Based on this multiresolution interpretation of airborne radar data processing, there appears to be an opportunity to develop detection techniques that attempt to optimize the signal processing resolution scale (e.g., length of temporal integration) to match the dynamics of a target of interest. This paper investigates signal processing techniques that exploit long CPIs to improve the detection performance of very slow-moving targets.

1. INTRODUCTION

A major goal of the Defense Advanced Research Projects Agency's Knowledge-Aided Sensor Signal Processing and Expert Reasoning (KASSPER) program [1–4] is to develop new techniques for detecting and tracking slow-moving surface targets that exhibit maneuvers such as stops and starts. Therefore, it is logical to assume that a combination of SAR and GMTI processing may offer a solution to the problem. SAR exploits very high spatial resolution via temporal integration and ownship motion to reduce the background clutter power in a given resolution cell to allow detection of nonmoving targets. GMTI radar, on the other hand, employs much lower-resolution processing but exploits relative differences in the space-time response between moving targets and clutter for detection. Therefore, SAR and GMTI represent two different temporal processing resolution scales which have typically been optimized and demonstrated independently to work well for detecting either stationary (in the case of SAR) or fast-moving (in the case of GMTI) targets.

Based on this multiresolution interpretation of airborne radar data processing, there appears to be an opportunity to develop detection techniques that attempt to optimize the signal processing resolution scale (e.g., length of temporal integration) to match the dynamics of a target of interest. For example, it may be beneficial to vary the signal processing algorithm as a function of Doppler shift (i.e., target radial velocity) such that SAR-like processing is used for very low Doppler bins, long coherent processing interval (CPI) GMTI processing is used for intermediate bins, and standard GMTI processing is used in the high Doppler bins. Figure 1 illustrates the concept. While not addressed in this paper, Figure 1 also suggests that varying the bandwidth as a function of target radial velocity may also be appropriate.

This paper explores signal processing techniques that "blur" the line between SAR and GMTI processing. We focus on STAP implementations using long GMTI CPIs as well as SAR-like processing strategies for detecting slow-moving targets. The performance of the techniques is demonstrated using ideal clutter covariance analysis as well as radar sample simulations and collected data. Discussion of multiresolution processing has been previously presented [5, 6]. In this paper, we augment the analysis with SAR-derived knowledge-aided constraints to improve performance in an environment that includes large discrete scatterers that induce elevated false-alarm rates.

Section 2 presents the details about the radar simulation used to analyze the signal processing algorithms. In Section 3, we consider the advantages of long CPIs using ideal covariance analysis. Section 4 introduces three adaptive

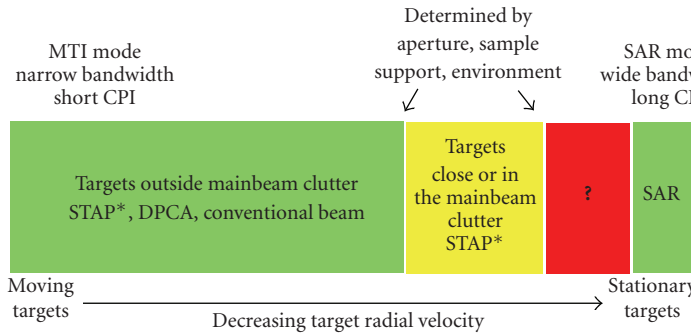

Figure 1: Illustration of multiresolution processing concept. The "$*$" indicates that the targets in the training data is an issue.

signal processing techniques that attempt to exploit long CPIs to improve the detection performance of very slow-moving targets. Section 5 presents performance results of the techniques using simulated and collected radar data. Finally, Section 6 summarizes the findings and outlines areas for further research.

2. GMTI RADAR SIMULATION

Simulated radar data was produced for use in analyzing the signal processing techniques proposed in this paper. Under previous simulation efforts [7–10] where the CPI length was short, it was possible to ignore certain effects due to platform motion during a CPI (e.g., range walk and bearing angle changes of the ground scattering patches). A description of the simulation methodology has been previously presented in [5, 6]. It is presented here also for completeness. Under the current effort, however, where we are specifically interested in long CPIs, it was important to produce simulated data that accurately accounts for the effects of platform motion. Therefore, the simulated data samples were computed as

$$x(k,n,m)=\sum_{p=1}^{P_c}\alpha_p t_{p,m} s\left(kT_s-\frac{r_{p,m}}{c}\right)e^{j(\phi_n(\theta_{p,m})-2\pi r_{p,m}/\lambda)}, \quad (1)$$

where k is the range bin index, $m=1,2,\ldots,M$ is the pulse index, $n=1,2,\ldots,N$ is the channel index, N is the number of spatial channels, M is the number of pulses, $s(t)$ is the radar waveform (LFM chirp compressed using a 30 dB sidelobe Chebychev taper), T_s is the sampling interval, λ is the radio wavelength, c is the speed of light, $r_{p,m}$ and $\theta_{p,m}$ are the two-way range and direction of arrival (DoA), respectively, for the pth ground clutter patch on the mth pulse, α_p is the complex ground scattering coefficient, $\phi_n(\theta_{p,m})$ is the relative phase shift of the nth array channel for a signal from DoA $\theta_{p,m}$, P_c is the number of clutter scatterers in the scene, and $t_{p,m}$ is a random complex modulation from pulse to pulse due to internal clutter motion (ICM) [11].

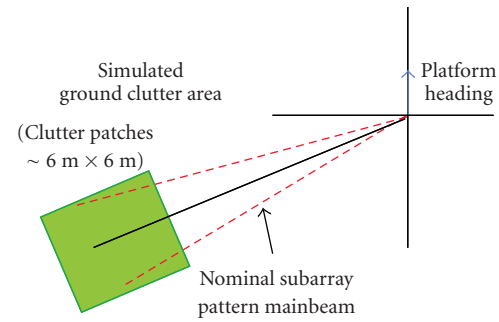

Figure 2: Simulation geometry.

The ideal clutter covariance matrix for a given range sample (i.e., range bin) is given as (e.g., [12])

$$\mathbf{R}_k=\sum_{p=1}^{P_c}|\alpha_p|^2\mathbf{v}_p\mathbf{v}_p^H\circ\mathbf{T}_{\text{icm}}, \quad (2)$$

where $\circ$ denotes the matrix Hadamard (elementwise) product and $\mathbf{v}_p$ is the $MN\times 1$ space-time response ("steering") vector [12] of the pth scattering patch. The elements of $\mathbf{v}_p$ are ordered such that the first N elements are the array spatial snapshot for the first pulse, the next N elements are the spatial snapshot for the second pulse, and so on. The elements of $\mathbf{v}_p$ are given as

$$v_p[N(m-1)+n]=s\left(kT_s-\frac{r_{p,m}}{c}\right)e^{j(\phi_n(\theta_{p,m})-2\pi r_{p,m}/\lambda)}. \quad (3)$$

Finally, we note that the matrix $\mathbf{T}_{\text{icm}}$ is a covariance matrix taper [13] that accounts for the decorrelation among the pulses due to ICM (i.e., due to $t_{p,m}$) and is based on the Billingsley spectral correlation model for wind-blown foliage decorrelation [14].

The simulation geometry is shown in Figure 2. The platform is flying north at an altitude of 11 km and the radar antenna is steered to look aft 17°. The clutter environment consists of an area at a slant range of 38 km that is slightly wider in the cross-range dimension than the antenna subarray pattern. The area is comprised of a grid of scattering

Table 1: Simulation parameters.

Parameter	Value (units)
Frequency	X-band
Bandwidth	10 MHz
PRF	1 kHz
Number of pulses	512
Antenna	3.5 m × 0.3 m
Number of subarrays	6 (50% overlap)
Subarray pattern	Hamming (∼ 40 dB sidelobes)
CNR	40 dB per subarray/pulse
Platform speed	125 m/s
Azimuth steering direction	17° re. broadside
Platform altitude	11 km ASL
Slant range	38 km

patches of dimension 6 m × 6 m. The complex amplitudes of the scattering patches are i.i.d. Gaussian with zero mean and variance that results in a clutter-to-noise ratio for a single subarray and pulse of approximately 40 dB at the slant range of 38 km. A list of system parameters is given in Table 1.

We note for this particular scenario that a given scattering patch in the mainbeam will "walk" on the order of one range resolution cell relative to the platform (due to platform motion) during the course of the 0.5-second CPI.

3. IDEAL COVARIANCE ANALYSIS

This section presents the results of GMTI system performance analyses as a function of CPI length using the ideal ground clutter covariance matrix.

3.1. Ground clutter cancellation

The ideal clutter covariance was used to investigate GMTI performance as a function of the CPI length using optimal space-time beamforming. The goal of this analysis was to establish an understanding of the theoretical advantages of using longer CPIs to detect moving targets. We employed a multi-bin post-Doppler space-time beamformer [15] with weights computed using the ideal clutter-plus-thermal-noise covariance matrix,

$$\mathbf{w}_o(\theta, f_d) = \left[\mathbf{H}^H(\mathbf{R}_k + \mathbf{R}_n)\mathbf{H}\right]^{-1}\mathbf{H}^H\mathbf{v}(\theta, f_d), \quad (4)$$

where $\mathbf{H}$ represents a matrix transformation of the space-time data into post-Doppler channel space (i.e., each column of $\mathbf{H}$ represents one of the adjacent Doppler filters), $\mathbf{R}_n$ is the covariance matrix of the thermal noise, and $\mathbf{v}(\theta, f_d)$ is the space-time response of a signal with DoA θ and Doppler shift f_d. We note that $\mathbf{v}(\theta, f_d)$ is the usual space-time steering vector [12] and does not include the effects of range walk. Also, in the SINR results, we do not account for the small losses that this will cause due to mismatch with a true target response.

Figure 3 shows the signal-to-interference-plus-noise ratio (SINR) loss as a function of CPI length for the cases with and without ICM. SINR loss is defined as the system sensitivity loss relative to the performance in an interference-free environment [12]. In this case, we have used 7 adjacent Doppler bins formed via orthogonal Doppler filters. It was found that using more Doppler bins resulted in negligible gain in performance. It is interesting to note that the shape of the filter response versus Doppler does not improve significantly as the CPI length is increased suggesting that the improvements in minimum detectable velocity (MDV) (i.e., the lowest radial velocities detectable by the system) will be modest for longer CPIs.

The curves in Figure 3 do not fully characterize the gain in system sensitivity with increasing CPI length given a constant power and aperture. Figure 4 shows the SINR for the cases shown in Figure 3, assuming that the interference-free SNR of the target using eight pulses in a CPI is 17 dB. Thus we see the effects on MDV of the increased sensitivity gain achieved by using more pulses (i.e., longer integration time). If we assume that 12 dB SINR is required for detection, then the MDV for each CPI length occurs when that curve intersects the SINR = 12 dB level.

Figure 5 indicates the MDV value as a function of the CPI length for the cases with and without ICM. We see that the gain in MDV drops off rapidly as the CPI length is increased. Therefore, we conclude that arbitrarily increasing the CPI will not result in significant gains in MDV beyond a certain point which will generally be determined by the system aperture size and ICM (or other sources of random modulations from pulse to pulse).

3.2. Targets in the secondary training data

While longer CPIs do not significantly improve the ability to resolve targets from clutter beyond a certain point due to the distributed Doppler response of ground clutter as observed by a moving airborne platform, there is the potential that longer CPIs will help better resolve targets in the scene. This has the obvious benefits of improving tracker performance by allowing clusters of closely spaced targets to be resolved.

An even greater potential benefit of the improved ability to resolve targets is that targets corrupting the secondary training data [9, 16] will be less likely to result in losses on other nearby targets. This is illustrated in Figure 6 where the SINR loss is shown for the case when a single target is injected into the ideal clutter covariance with a target radial velocity of 3.9 m/s. We see that as the CPI length is increased the region incurring losses due to the target in the covariance gets increasingly narrow indicating that it will only take a very small relative Doppler offset between two targets to avoid mutual cancellation. Quantifying the effectiveness of longer CPIs in mitigating the problem of targets in the secondary training data for *realistic* moving target scenarios is an area for future research.

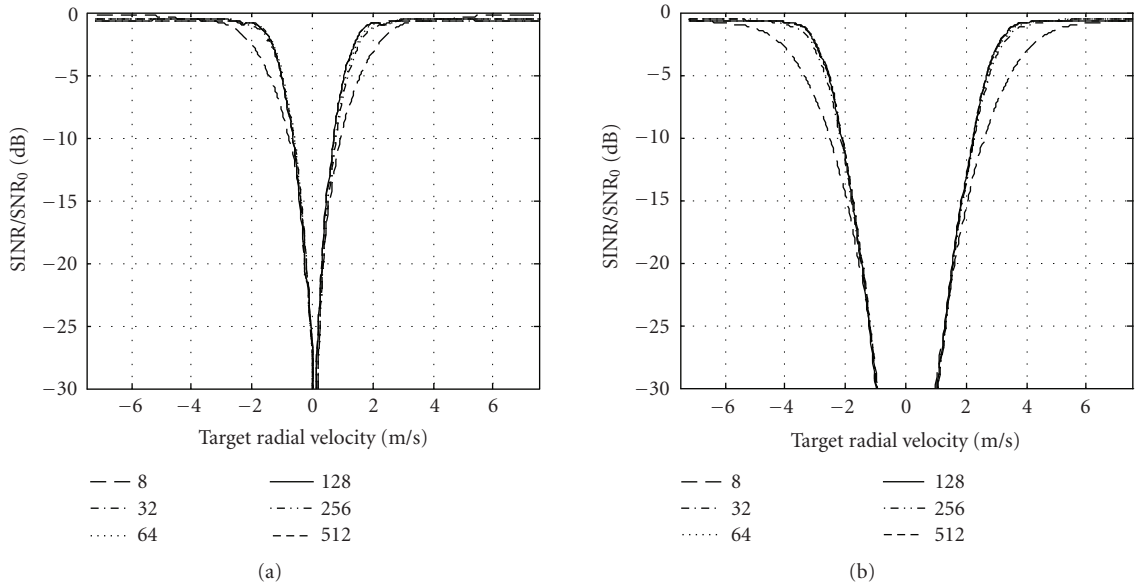

Figure 3: Optimal SINR loss. (a) No ICM. (b) Billingsley ICM. The legend indicates the number of pulses used in a CPI.

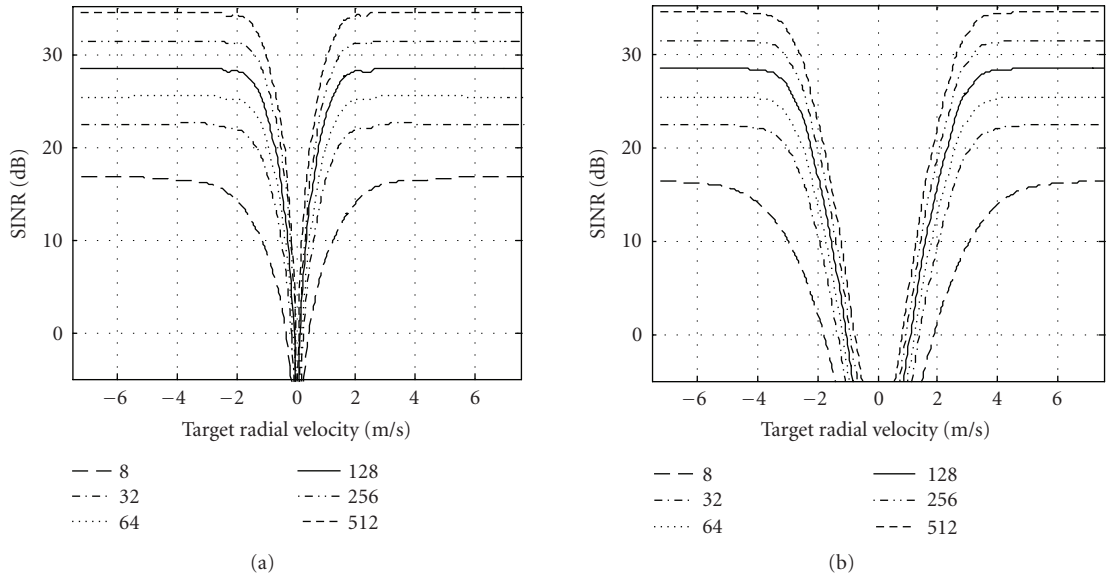

Figure 4: Optimal SINR assuming eight-pulse SNR is 17 dB. (a) No ICM. (b) Billingsley ICM. The legend indicates the number of pulses used in a CPI.

4. ADAPTIVE ALGORITHMS

This section details three adaptive signal processing algorithms that exploit long CPIs to improve the detection performance of very slow-moving targets. The goal is to evaluate the utility of long CPIs for performance improvements including evaluating the hypothesis that longer CPI data may be exploited to increase the number of samples available for covariance estimation without significantly increasing the range swath over which samples are drawn. It is assumed that this will be advantageous in realistic clutter environments where variations in the terrain and land cover often limit the stationarity of the radar data in the range dimension to narrow regions.

4.1. Sub-CPI processing

The ideal covariance matrix analysis presented in Section 3.1 suggests that for a given system it may not be necessary to coherently process all the pulses in a long CPI to approach

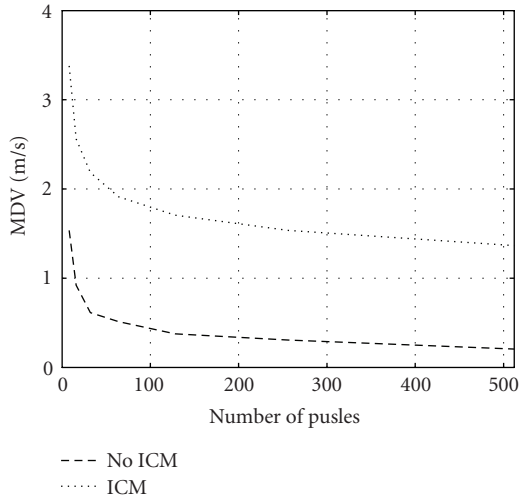

Figure 5: MDV based on the curves shown in Figure 4.

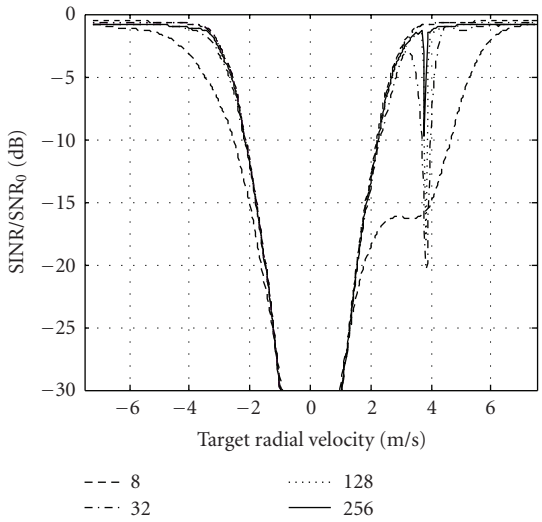

Figure 6: Optimal SINR loss for the case when a single target corrupts the secondary training data. The target corrupting the training data has a target radial velocity of approximately 3.9 m/s. The legend indicates the number of pulses used in a CPI.

the optimal MDV. Therefore, if many pulses are available, it may be advantageous to limit the coherent processing interval, but exploit the extra pulses to increase the training data set for covariance estimation. It is important to note that the potential advantage of reducing effects due to targets in the training data will not be realized in this case since the *coherent* processing interval is still short. For example, Figure 7 illustrates an approach for segmenting the pulses to form data snapshots that can be used for covariance matrix estimation. In this case, the sample covariance matrix is computed as

$$\hat{\mathbf{R}} = \frac{1}{KK'} \sum_{k=1}^{K} \sum_{k'=1}^{K'} \mathbf{x}_{k,k'} \mathbf{x}_{k,k'}^{H}, \tag{5}$$

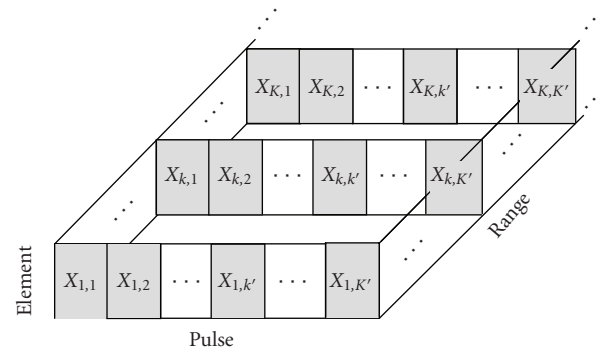

Figure 7: Illustration of sub-CPI segmentation.

where $\mathbf{x}_{k,k'}$ is the snapshot from the kth range bin and k'th sub-CPI. We note that vector $\mathbf{x}_{k,k'}$ is formed by reordering the matrix $\mathbf{X}_{k,k'}$ as shown in Figure 7 so that the first N elements are the spatial samples on the first pulse, the next N elements are the spatial samples on the second pulse, and so on. The quantity K is the number of training range samples and K' is the number of sub-CPIs used in the training. The effect of varying these quantities is demonstrated in Section 5.

The covariance estimate based on the sub-CPI data is used to compute an adaptive weight vector that can generally be applied to each of the sub-CPIs in the range bin under test to form K' complex beamformer outputs. Methods for combining these outputs either coherently or incoherently to improve the system sensitivity are an area for future research. It is worth noting, however, that in general it should be possible to coherently combine the outputs if unity gain constraints are employed in the beamformer calculation and delays in the target response in each sub-CPI relative to the start of the CPI are accounted for.

While this approach is interesting from a theoretical point of view in that it shows an alternative approach for exploiting a long CPI to increase training samples without increasing the training window, it was found to be difficult to implement in practice. This is due to the fact that when used to achieve highly localized training, this technique exacerbates the problem of target self-nulling due to the range sidelobe contamination of the training data. Also, we would not expect the sub-CPI training approach to help mitigate the problem of targets in the training data since the coherent processing will still occur over a short CPI.

4.2. Long-CPI post-Doppler

An alternative approach to sub-CPI processing is to Doppler process (e.g., discrete Fourier transform) the CPI using all the pulses and then apply adaptive techniques similar to multi-bin post-Doppler STAP [15]. In the case when the CPI is very long, it may be advantageous to employ SAR processing (instead of Doppler processing) that accounts for range walk of the scatterers in the scene that results from platform motion. This approach has been proposed previously [17]. Figure 8 illustrates the concept. We note that this technique will take advantage of the property of long CPIs to reduce

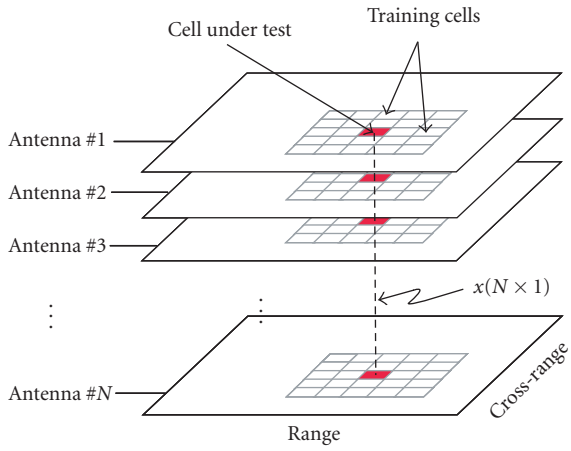

Figure 8: Illustration of long-CPI post-Doppler processing. Note training is possible in both range and cross-range.

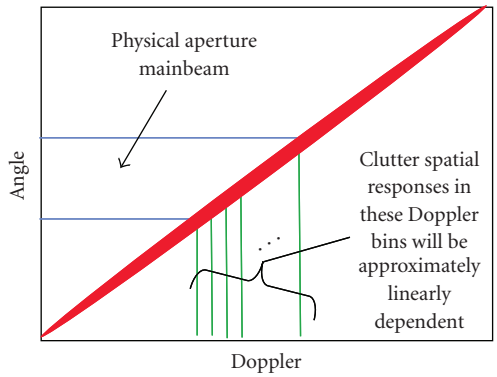

Figure 9: Illustration of clutter ridge and large difference in angular and temporal resolution for long CPIs.

the effects of targets in the secondary training data as long as multiple adaptive Doppler bins are employed.

In the simplest form, the data from each antenna is used to form a spatial-only covariance matrix estimate using data from Doppler and range bins (or cross-range and range pixels in the case of SAR preprocessing). If we only employ data from adjacent range bins for training, this technique (in the case of Doppler processing) is identical to factored time-space beamforming [12] (i.e., single-bin post-Doppler adaptive processing). In [17] it was proposed that adjacent cross-range (or Doppler bins) should also be included in the training set. This may at first seem unusual in the context of GMTI STAP for which training using only adjacent range bins is the common practice.

Figure 9 illustrates why it is efficacious to use data from adjacent Doppler bins to estimate the correlation among the spatial channels when the CPI is long.

We see that since the Doppler resolution is much finer than the spatial resolution, clutter patches in adjacent Doppler bins will have highly linearly dependent spatial responses and therefore can be averaged to improve the spatial covariance matrix estimate [5, 6]. The azimuth beamwidth

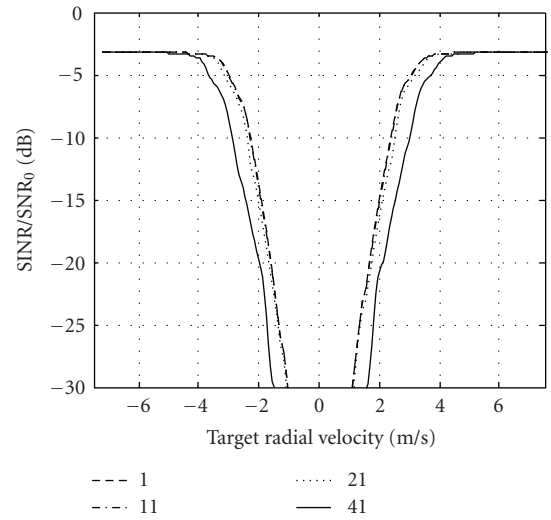

Figure 10: Effect of Doppler training region size in long-CPI post-Doppler processing. The training bins are centered around and include the bin under test. The legend indicates the number of Doppler training bins used.

of the physical aperture is given as

$$\delta_a = \frac{\lambda}{L}, \tag{6}$$

where L is the length of the aperture in the horizontal dimension. The azimuth beamwidth of the synthetic aperture (azimuthal extent of the ground clutter in a single Doppler bin) is given as [18]

$$\delta_d = \frac{\lambda}{2L_{\text{eff}}} = \frac{\lambda f_P}{2v_p M}, \tag{7}$$

where L_{eff} is the distance traveled by the platform during the CPI, f_p is the PRF, and v_p is the platform speed. The ratio of δ_a to δ_d,

$$f_{\text{res}} = \frac{\delta_a}{\delta_d} = \frac{2v_p M}{L f_p}, \tag{8}$$

gives an approximate expression for the number of Doppler bins within the mainbeam and thus the number of adjacent Doppler bins that can be used as training samples. For the system simulation discussed in Section 2, the quantity $f_{\text{res}} = 36.6$.

Figure 10 demonstrates the effects of increasing the number of adjacent Doppler bins used in the training set for the single adaptive bin case (i.e., factored time-space adaptive beamforming). The total number of pulses in the CPI is 256 which results in $f_{\text{res}} = 18.2$ and we note that a 65 dB sidelobe level Chebychev taper is applied across the 256 pulses prior to Doppler processing. In this example, the ideal spatial-only covariance matrix for each of the adjacent Doppler bins used in the training strategy was computed and then summed together to form the "ideal" (ensemble average of the) estimated covariance matrix. This covariance matrix,

which takes into account the effects of training over adjacent Doppler bins, was then used to compute SINR loss. As expected, when the number of bins exceeds $f_{\text{res}} = 18.2$, the SINR loss begins to degrade.

More sophisticated versions of the long-CPI post-Doppler algorithm will include multiple temporal degrees of freedom. In [17] multiple adjacent SAR pixels were combined adaptively along with the spatial channels to form the adaptive clutter filter. When training samples are only chosen from adjacent range bins, this version of the algorithm is similar to multi-bin post-Doppler element-space STAP [15]. In fact, if the preprocessing uses Doppler filters instead of SAR processing, the algorithm is mathematically equivalent to multi-bin post-Doppler STAP.

Choosing training samples from adjacent Doppler and range bins is not as straightforward as it was in the single adaptive bin case since the samples can be chosen to be either overlapped or nonoverlapped in Doppler. In [17] it was observed that the multipixel covariance estimation process introduced "artificial" increases in the correlation of the background thermal noise between pixels when the overlapped training samples were used since the thermal noise for two overlapping training samples will typically be correlated. Theoretical analysis of estimators that use overlapping training data to estimate the multipixel correlation matrix is an area for future research.

4.3. SAR-derived knowledge-aided constraints

In [19–22] the application of knowledge-aided constraints was developed. In that analysis, the ground clutter is assumed to be known to some degree and the interference covariance matrix is assumed to be the sum of three components: a known clutter covariance component, an unknown clutter covariance component, and thermal noise, typically uncorrelated among the channels and pulses. This structure is used to derive a post-Doppler channel-space weight that incorporates the known clutter covariance component as a quadratic constraint. The approach to finding the optimal weight vector for the mth channel $\mathbf{w}_m$ is to solve the following constrained minimization:

$$\min_{\mathbf{w}_m} E\left[\left|\mathbf{w}_m \mathbf{x}_m\right|^2\right] \quad \text{such that} \quad \begin{cases} \mathbf{w}_m \mathbf{v}_m = 1, \\ \mathbf{w}_m^H \mathbf{R}_{c,m} \mathbf{w}_m \le \delta_{d,m}, \\ \mathbf{w}_m^H \mathbf{w}_m \le \delta_{l,m}, \end{cases} \tag{9}$$

where for a desired reduced-DoF orthonormal $MN \times D$ ($D < MN$) transformation $\mathbf{H}_m$, we have

$$\begin{aligned} \mathbf{x}_m &= \mathbf{H}_m^H \mathbf{x}, & \mathbf{v}_m &= \mathbf{H}_m^H \mathbf{v}, \\ \mathbf{R}_{c,m} &= \mathbf{H}_m^H \mathbf{R}_c \mathbf{H}_m, & \mathbf{R}_m &= \mathbf{H}_m^H \hat{\mathbf{R}}_{\mathbf{xx}} \mathbf{H}_m, \end{aligned} \tag{10}$$

and where $\mathbf{R}_c$ represents the known component of the interference (e.g., (2)), $\hat{\mathbf{R}}_{\mathbf{xx}}$ is the usual sample estimate of the covariance matrix, and $\delta_{d,m}$ and $\delta_{L,m}$ are arbitrarily small constants.

In (9), the first constraint is the usual point constraint [12] while the third constraint introduces diagonal loading to the solution. The second constraint incorporates a priori knowledge into the solution by forcing the space-time weights to tend to be orthogonal to the known clutter subspace. The result, derived in [21, 22], is

$$\begin{aligned} \mathbf{w}_m &= \frac{\left(\mathbf{R}_m + \beta_{d,m}\mathbf{R}_{c,m} + \beta_{L,m}\mathbf{I}_D\right)^{-1}\mathbf{v}_m}{\mathbf{v}_m^H\left(\mathbf{R}_m + \beta_{d,m}\mathbf{R}_{c,m} + \beta_{L,m}\mathbf{I}_D\right)^{-1}\mathbf{v}_m} \\ &= \frac{\left(\mathbf{R}_m + \mathbf{Q}_m\right)^{-1}\mathbf{v}_m}{\mathbf{v}_m^H\left(\mathbf{R}_m + \mathbf{Q}_m\right)^{-1}\mathbf{v}_m}, \end{aligned} \tag{11}$$

where $\mathbf{Q}_m = \beta_{d,m}\mathbf{R}_{c,m} + \beta_{L,m}\mathbf{I}_D$, $\mathbf{I}_D$ is a $D \times D$ identity matrix, and $\beta_{d,m}$ and $\beta_{L,m}$ are the colored and diagonal loading levels, respectively, that may be specific to each transformation. Note that $\beta_{d,m}$ and $\beta_{L,m}$ are related to the constraint values $\delta_{d,m}$ and $\delta_{L,m}$ via two coupled nonlinear inequality relations [22].

It is interesting to note that the solution given in (11) results in a "blending" of the information contained in the sample covariance matrix and the a priori clutter model. Therefore, the solution has the desirable property of combining adaptive and deterministic filtering. In fact, the solution will provide beampatterns that are a mix between the fully adaptive pattern, a fully deterministic filter, and the conventional pattern represented by the constraint $\mathbf{v}_m$. An interesting area for future research will be to develop rules for setting the covariance "blending" factors based on the characteristics of the operating environment (e.g., expected density of targets, terrain type, etc.) derived from auxiliary databases. Additional discussion regarding the selection of the loading levels may be found in [19].

We note that the beamformer weights in (11) can be re-written to permit interpretation as a two-stage filter where the first stage "whitens" the data vector using the a priori covariance model and then is followed by an adaptive beamformer based on the whitened data [19]. This leads us to consider the possibility of using SAR data to identify discrete scatterers, generate a space-time response for that discrete scatterer using the observed spatial response and a predicted temporal response, and using that response to build a prefilter/colored-loading matrix to minimize the false-alarm impact of the discrete scatterers in a given scenario. This process is illustrated in Figure 11 and described in more detail in [22].

5. RESULTS

The simulated data discussed in Section 2 along with experimentally collected data was used to test the adaptive processing techniques described in Section 4. Five range samples were simulated and an ideal covariance matrix for the center range bin was generated. Adaptive weights were estimated from the data samples using the various training strategies and then (for the simulated data) applied to the ideal covariance matrix to compute the SINR loss metric.

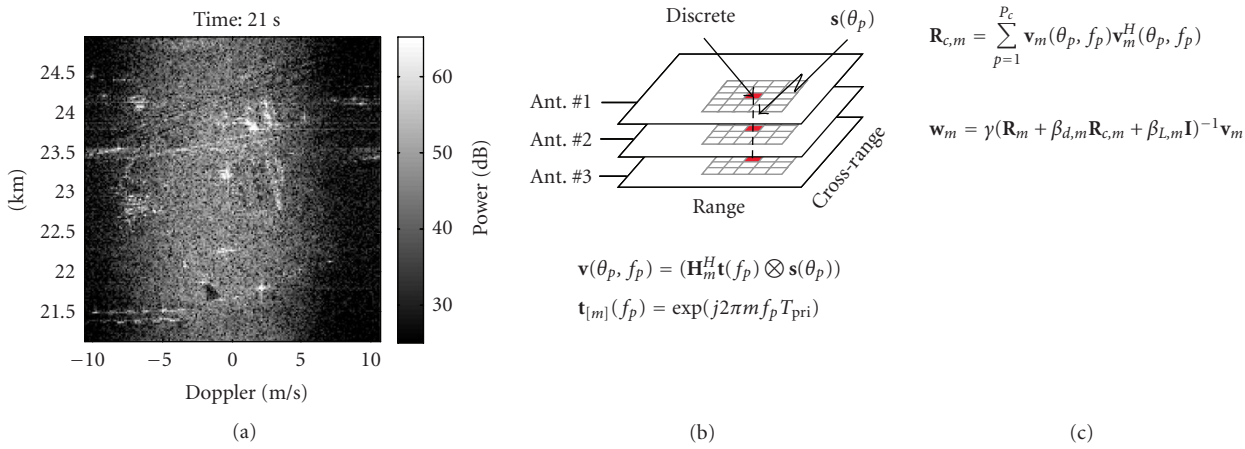

Figure 11: SAR-derived colored-loading processing algorithm. (a) Step 1: threshold "low-resolution" SAR map to detect discrete clutter. (b) Step 2: form space-time response for each discrete and transform to post-Doppler space (use observed spatial response). (c) Step 3: use response to form a range-dependent "loading" matrix for each Doppler bin, add to sample covariance, and run STAP processor.

5.1. Sub-CPI processing

Figure 12 shows the SINR loss for sub-CPI processing as a function of the number of pulses in the sub-CPI for three cases: (1) range-only training, (2) sub-CPI only training, and (3) range and sub-CPI training. The adaptive algorithm was multi-bin post-Doppler channel-space STAP employing three adjacent adaptive Doppler bins. Diagonal loading with a level of 0 dB relative to the thermal noise was used in all cases.

We see that range-only training results in poor performance since there are too few training samples to support the adaptive DoFs. Performance is improved by using the sub-CPIs from a single range bin as the training data. In this case, the number of training samples is equal to the total number of pulses (512) divided by the number of pulses in the sub-CPI. Thus, for the examples shown, the number of sub-CPI training samples is 64, 32, and 16 for the 8, 16, and 32 pulse sub-CPI cases, respectively.

Finally, we see that if training samples are chosen from both sub-CPIs and range bins, we get near-optimal (relative to the ideal covariance case) performance. In this case, the total number of training samples is the number of range bins multiplied by the number of sub-CPI segments. Thus the number of samples for the cases shown is 320, 160, and 80 for the 8, 16, and 32 pulse sub-CPI cases, respectively. This example demonstrates that highly localized training regions in range may be possible if training data is augmented with sub-CPI data snapshots. This strategy will generally be the most advantageous in nonhomogeneous clutter environments.

5.2. Long-CPI post-Doppler

Figure 13 shows the SINR loss results for the long-CPI post-Doppler processing technique. The results are presented for three cases: (1) a single adaptive Doppler bin, (2) three adjacent adaptive Doppler bins with *overlapped* Doppler training snapshots, and (3) three adjacent adaptive Doppler bins with *nonoverlapped* Doppler training snapshots. In each case, the CPI length is 512 and training data from 21 adjacent Doppler filters is used in the covariance estimation. In this case, $f_{\text{res}} = 36.6$, but a value of 21 was used to ensure that no losses were incurred due to overextending the Doppler training window. We also note that the single adaptive Doppler bin case employs a 65 dB sidelobe level Chebychev taper across the 512 pulses prior to Doppler processing.

Figure 13(a) ("1 adaptive bin") has a black dashed curve which represents the case when five range samples are used to estimate the spatial covariance matrix which in this case has dimension six due to the six spatial channels employed in the simulation. We note that diagonal loading at a level of 0 dB relative to the thermal noise floor was required so the estimated covariance matrix could be inverted. We see that the range-only training results in poor performance due to the small number of training samples.

We see, however, that when adjacent Doppler bins are used for training, we get much better performance (dotted and dash-dotted curves). The dotted curve uses adjacent Doppler bins and five range samples for training data and the dash-dotted curve uses adjacent Doppler bins from a single range bin. We see that the best performance is achieved when multiple adaptive Doppler bins are employed and training is performed using both adjacent range bins and overlapping Doppler samples. The generally poor performance when only adjacent Doppler samples are used is most likely attributed to the correlation of the thermal noise among the training samples which results in a poor estimate of the background thermal noise statistics. Developing a better understanding of this phenomenon via analysis and simulation is an area for future research.

The data set was generated both with and without targets so clutter-only training data is available for use in analyzing

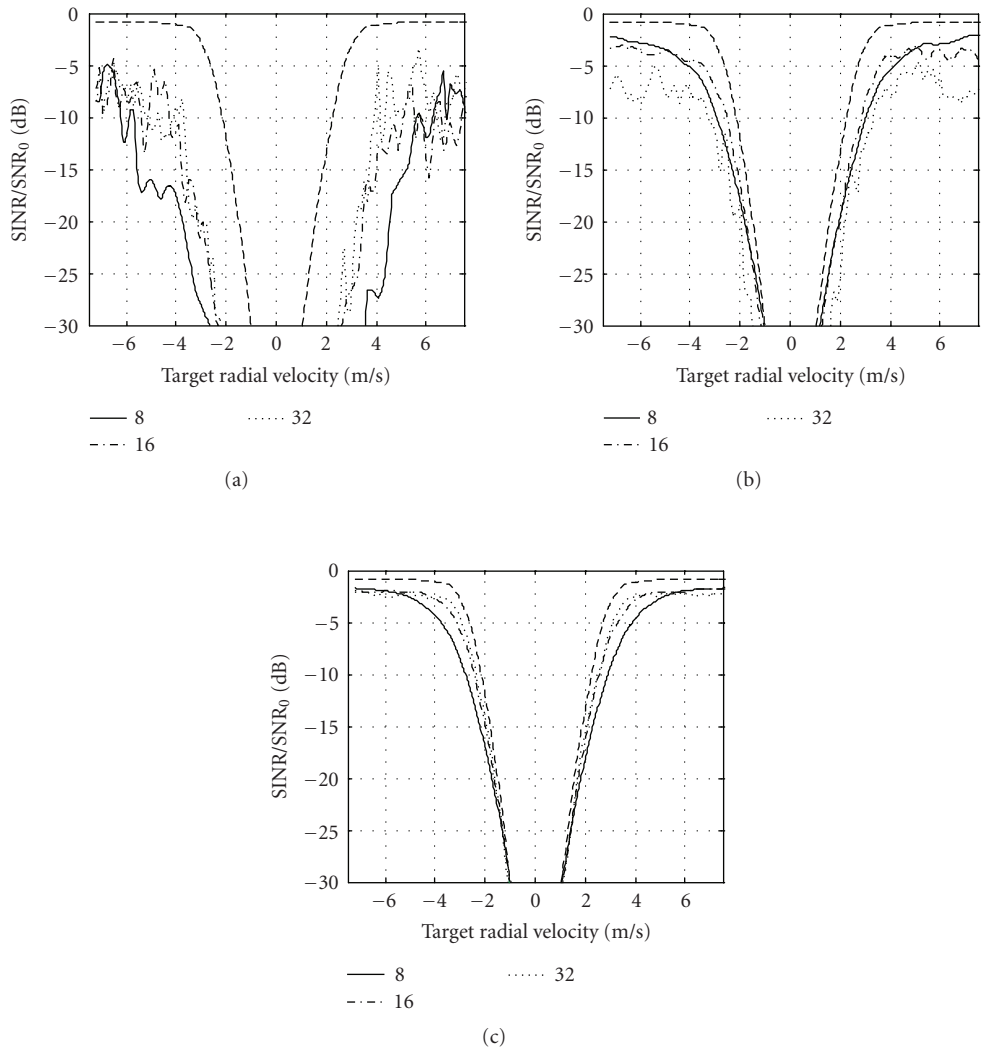

FIGURE 12: SINR loss for sub-CPI training. (a) Range-only training (five range bins). (b) Training using sub-CPIs from a single range bin. (c) Training using sub-CPIs from five range bins. The black dashed line is the optimal full-DoF STAP performance. The legend indicates the number of pulses used in a CPI.

algorithms. For example, the clutter-only training data can be used to compute adaptive weights and can then be applied to the clutter-plus-targets data. This allows us to isolate the effects of targets corrupting the secondary training data. Figure 14 shows the beamformer output for three-bin post-Doppler STAP with 48 training samples chosen in the range dimension only. Also shown is an overlay of ground truth targets. The result is shown for a 64-pulse CPI and a 256-pulse CPI. We see that when clutter-only training data is used for training, both the 64-pulse and 256-pulse CPIs detect the same targets including the very slow movers near the clutter ridge (0 m/s Doppler). When the clutter-plus-targets training data is used, however, the 256-pulse CPI detects significantly more targets for the reasons discussed in Section 3.2. We note that more than 256 pulses (0.25-second CPI) were not used to avoid significant losses due to range and Doppler walk. In cases when longer CPIs than shown here are employed, more sophisticated preprocessing steps than simple Doppler processing will be required (e.g., SAR image formation).

Figure 15 summarizes the number of detections as a function of threshold level (relative to thermal noise) for three values of the CPI length. We note that the threshold values shown are for the 64-pulse case and that the threshold values for the 128- and 256-pulse cases were increased by 3 dB and 6 dB, respectively, to account for the increased integration gain. Threshold crossings were declared detections if they were within a single range and Doppler bin of a target in the ground truth. We see that when clutter-only data is used for training, each CPI length produces approximately the same number of detections. When the targets are included in the training, however, the longer CPI results in a significant increase in detections. We note that there are a total of 38 targets in the scenario.

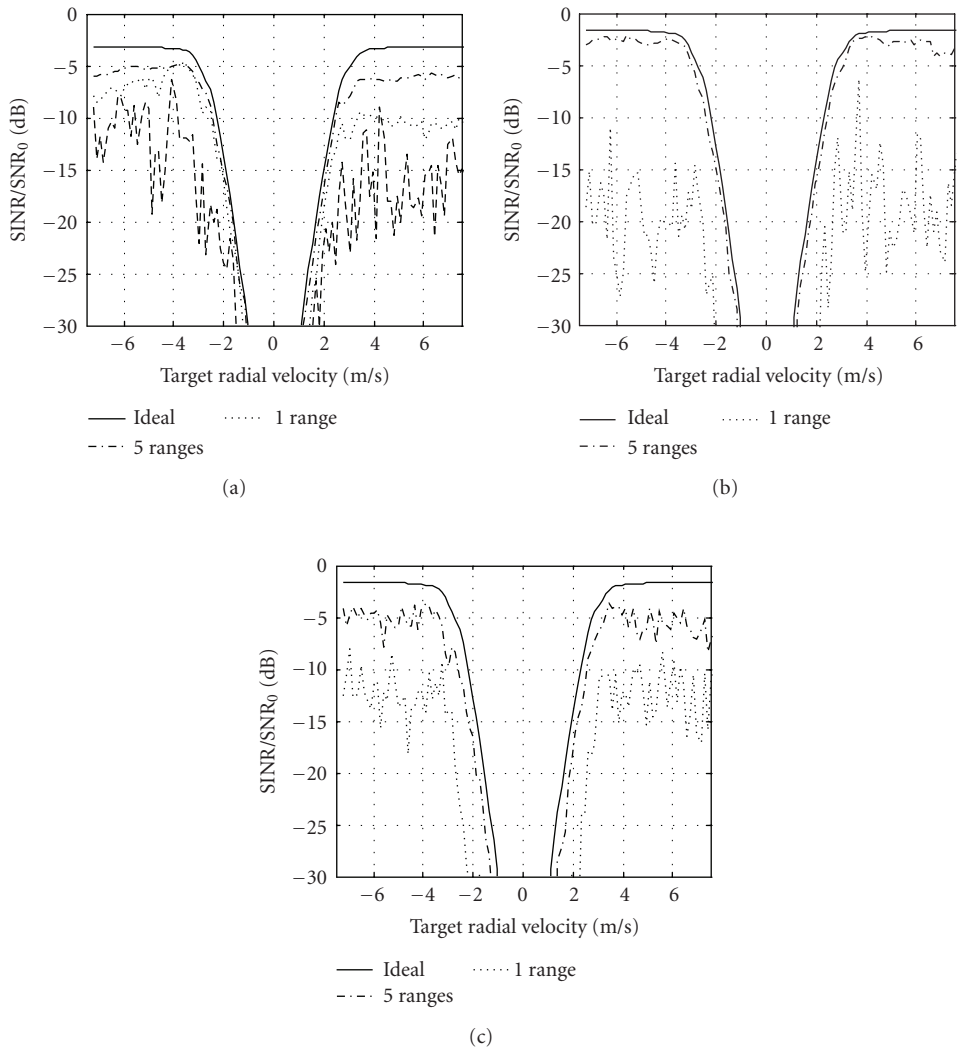

Figure 13: Long-CPI post-Doppler processing. (a) One adaptive bin (factored post-Doppler). The black dashed line indicates range-only training. (b) Three adaptive bins (multi-bin post-Doppler) with *overlapped* training. (c) Three adaptive bins with *nonoverlapped* training. legend indicates either ideal covariance matrix result or number of ranges used in training.

Figure 16 shows the beamformer output for the case when training data from adjacent Doppler bins is employed. In this case, a single three-bin sample was chosen on each side of the bin under test in the Doppler dimension (we are still using three-bin post-Doppler STAP) separated by three bins from the bin under test over a range swath of 24 samples. Thus the extra training samples chosen in the Doppler dimension are nonoverlapping and the total number of training samples is 48. We see that even in the clutter-only training case that the response of the very slow-moving targets near 0 m/s Doppler are somewhat weaker than in the range-only training case (Figure 14(a), 256 pulse case) indicating that this method of training tends to reduce the ability to resolve slowly moving targets from clutter.

In the clutter-plus-targets training case, we see that in some cases this method of training improves performance (compare to Figure 14(b), 256 pulse case). For example, since this method does not use training samples from the same Doppler bin versus range, the two targets at approximately 45.25 km range that are closely spaced in Doppler are detected whereas in Figure 14(b) they are not. However, there are several targets detected in Figure 14(b) that are not detected in Figure 16(b). Even though the targets corrupting the training data are in a different Doppler bin (since the training samples are chosen from adjacent Doppler bins), across the three chosen bins their response is very similar to the 3-bin response of the target of interest. Thus they can still contribute to nulling a target of interest.

An interesting difference between the range-only training and adjacent Doppler training results is a noticeable reduction in the amount of undernulled clutter, particularly around the clutter ridge. This indicates that the more localized training (the training range swath here is 360 m as opposed to 720 m in Figure 14) as well as the inclusion of the

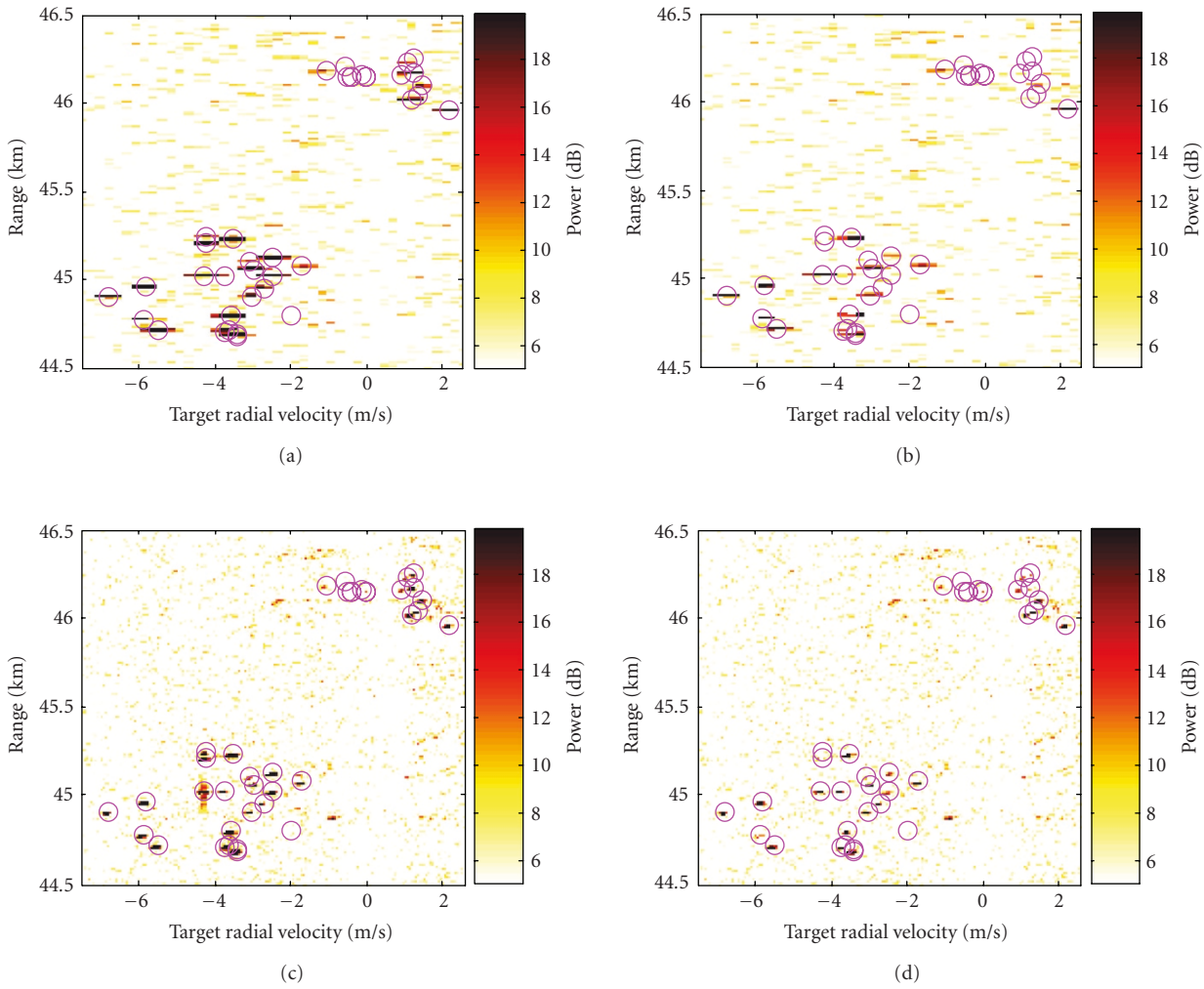

FIGURE 14: Beamformer output for range-only training. (a) and (c) represent clutter-only training data for 64 and 256 pulses, respectively. (b) and (d) represent clutter-plus-targets training data for 64 and 256 pulses, respectively. Magenta circles are ground truth. Mainbeam clutter at 0 m/s.

range bin of interest in the training set results in improved clutter cancellation performance which is the expected result.

5.3. SAR-derived knowledge-aided constraints

The Tuxedo radar is a data collection platform with an X-band system with a three-phase center antenna array. The system collects very long CPIs (greater than ten seconds) that can be used to form multiaperture synthetic aperture radar images. For the examples shown in this paper, only a subset of the pulses spanning a more typical GMTI CPI (less than 0.5 second) was used. The data set was collected at Camp Navajo, Ariz, in a desert environment exhibiting very little terrain relief.

The scenario does include significant strong clutter discretes scatterers, however, due to various man-made structures (buildings, towers, etc.). For example, Figure 17(a) shows the range-Doppler map for the beamformer output for a single azimuth steering direction. We clearly see the mainbeam clutter which generally consists of benign underlying ground clutter plus large discretes in various range bins. This type of environment can cause problems for STAP since omitting the range bin under test from the covariance matrix estimate can lead to severe undernulled clutter. This situation can be addressed using the technique described in Section 4.3.

A long GMTI CPI (or "low-resolution SAR") image was formed such as the one in Figure 17(a) and thresholded to extract the largest discretes. Figure 17(b) shows the 254 discretes extracted from the Tuxedo data by applying a 70 dB threshold to the image in Figure 17(a). We note that this general approach has been previously proposed [23], however, this implementation varies significantly in that it uses the colored-loading framework and includes an automatic calibration scheme. We also note that target cancellation will in general be avoided since the target-to-clutter ratio is expected to be low for the chosen long CPI range-Doppler processing output.

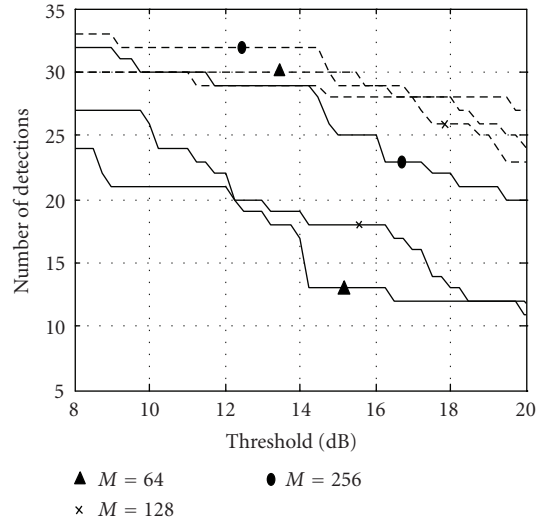

Figure 15: Number of detections. The threshold values shown are for the 64-pulse case. The solid lines represent the clutter-plus-targets training and the dashed lines represent the clutter-only training.

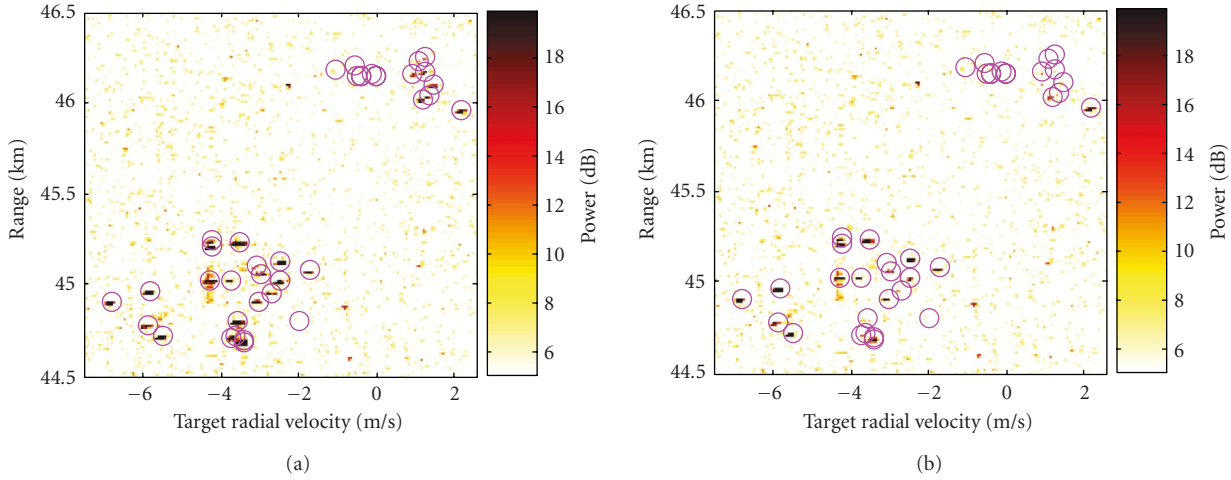

Figure 16: Post-Doppler STAP with training over adjacent Doppler bins. (a) Clutter-only training for 256 pulses. (b) Clutter-plus-targets training for 256 pulses. Magenta circles are ground truth.

Figure 18 compares the beamformer output for conventional and KA-STAP using the data-derived colored-loading matrices discussed above. The information used in the loading matrices was derived from a 0.4-second CPI and applied to a 0.1-second CPI. This result is an example of multitemporal resolution processing. Both the STAP and KA-STAP results use a multi-bin post-Doppler element-space algorithm with three bins and three channels (nine DoFs). The number of training samples was 200 with the bin under test and three guard bins on each side of the bin under test excluded from the training set. In both cases, there is diagonal loading that is approximately equal to the thermal noise level and for the KA-STAP case the maximum eigenvalue of the colored-loading matrix of the Doppler domain colored-loading matrix is approximately 30 dB above the thermal noise level. Finally, we note that the computed beamforming weights in all cases have been normalized to give unit gain on white noise.

We see that many of the "streaks" in the conventional STAP result (see arrow markers on the plot) caused by undernulling of the strong discretes have been eliminated in the KA-STAP result. The conclusion is that by including data-derived knowledge of the discrete locations and their spatial responses in the KA-STAP approach will lead to significantly fewer false alarms and/or improved detection sensitivity than conventional STAP.

Thirty-five GMTI CPIs were generated from the 40 000 pulses of coherent Tuxedo data by taking a block of pulses every second. GMTI CPIs consisting of 128 pulses (approximately 100 milliseconds) and 32 pulses (approximately 25

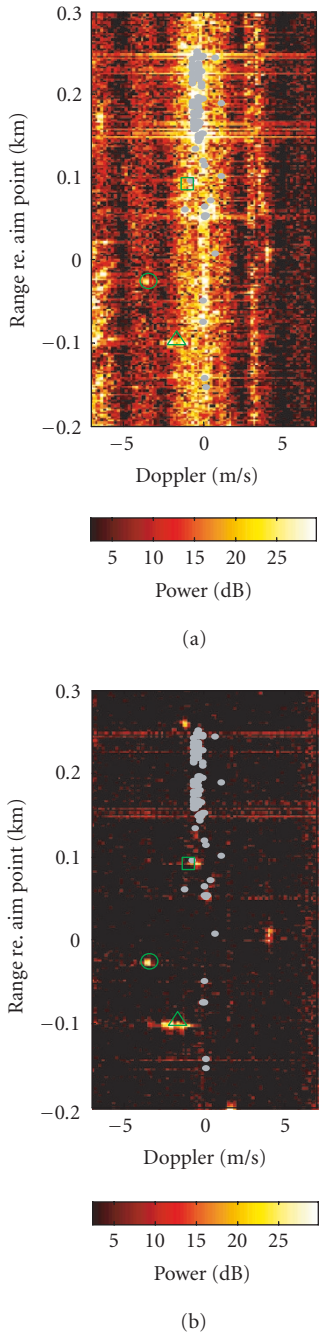

Figure 17: A portion of the Tuxedo beamformed range-Doppler clutter map ("low-resolution SAR") for Camp Navajo, Ariz. (a) Low-resolution SAR map with an overlay of "detected" clutter discretes (dark grey dots) used to form the colored-loading matrix. (b) STAP beamformer output with same overlay of discretes. CPI length is 0.4 second. The markers are the locations of GPS-instrumented ground targets.

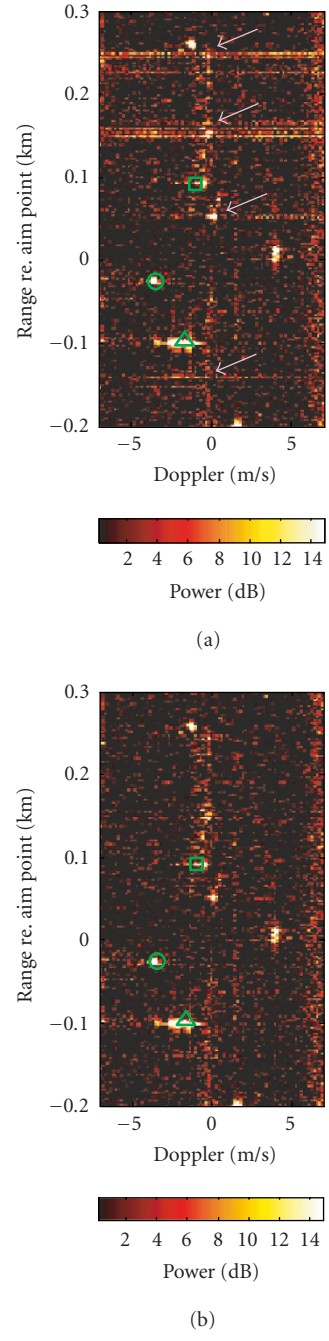

Figure 18: Comparison of beamformer output for Tuxedo data. (a) Traditional STAP. (b) STAP with colored loading. Arrows mark some of the clutter discretes that lead to undernulled clutter in the traditional STAP case.

milliseconds) were considered. The radial velocities of two of the targets, a five-ton truck and an HMMWV, are plotted over time in Figure 19. We note that at 15 seconds and approximately 32 seconds, the two target radial velocities coincide (i.e., both are in the same Doppler bin).

Now consider, for a 25-millisecond CPI using the algorithm of Figure 11, the target beamformer output power as a function of time (CPI). Two training window sizes were used, 200 m and 60 m. The larger window size results in one of the targets being included in the training set of the other

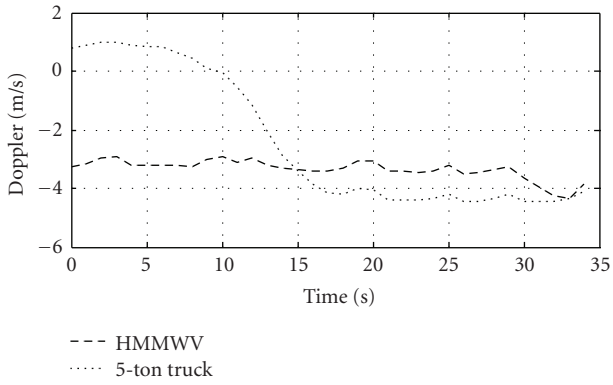

Figure 19: Target radial velocity as a function of time.

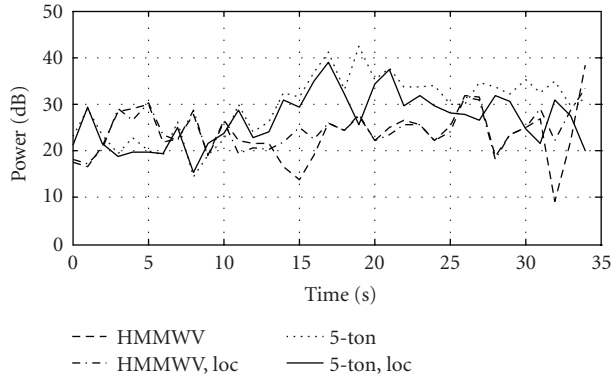

Figure 20: Beamformed target power using knowledge-aided STAP and a 25-millisecond CPI. The shorter training window (60 m) is indicated by "loc."

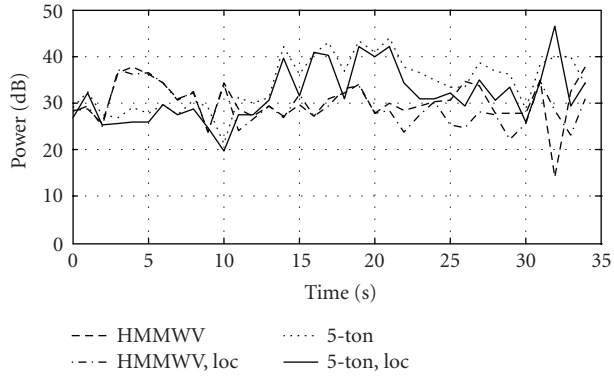

Figure 21: Beamformed target power using knowledge-aided STAP and a 100-millisecond CPI. The shorter training window (60 m) is indicated by "loc."

and vice versa (e.g., the HMMWV is included in the training for the range bin corresponding to the five-ton truck) while this does not result with the smaller training window. The beamformed target output power is shown in Figure 20 as a function of time. We see that when the two target radial velocities coincide, there is a significant reduction in the target power out of the beamformer for the HMMWV when using the larger training window. The shorter training window does not result in the same effect. We note that the same does not happen with the five-ton truck. This is most likely due to the lower power of the HMMWV.

A 100-millisecond CPI was also analyzed. The results are shown in Figure 21. Similar effects are observed at time 32 seconds as were observed in Figure 20. However, at time 15 seconds the same reduction in beamformed target power does not result for the larger training window. This is most likely due to the spreading across multiple Doppler bins that occurs with the five-ton truck. This spreading results from the radial acceleration that is observed for that vehicle in Figure 19.

6. SUMMARY

The concept of using long CPIs to improve the detection of very slow-moving targets was investigated. The concept was motivated by observing that airborne radars use short CPIs to detect fast-moving targets (e.g., GMTI STAP) and very long CPIs to detect stationary targets (e.g., SAR) so that it is logical to assume that it may be advantageous to use longer and longer CPIs as the assumed Doppler velocity of targets of interest is decreased.

Theoretical analysis of optimal beamforming techniques that cancel clutter (e.g., STAP) was used to demonstrate that for a given system and operating environment, there is a CPI length beyond which significant improvements in MDV diminish. Beyond the cutoff, the width of the antenna and phenomenology such as ICM limit the MDV performance. It was postulated, however, that the problem of targets corrupting the training data may be significantly reduced since when the CPI is long, it will require only a very small relative difference in Doppler velocity between targets to cause enough decorrelation so that when they corrupt the training data, the resulting sensitivity losses are negligible.

While the improvements of optimal beamformers in detecting very slow-moving targets tend to diminish beyond a certain CPI length, *adaptive* implementations of the optimal beamformers may benefit significantly from longer CPIs. Two adaptive techniques were presented that take advantage of the longer CPI to improve the convergence properties of the beamformer solution and thus increase the performance of the beamformer. It was shown that these techniques can reduce the number of adjacent range samples required for training which will generally improve performance in realistic clutter environments where the stationarity of the ground clutter is often limited to narrow range regions due to significant terrain relief and land cover variations.

Finally, the use of ownship SAR to identify discrete scatterers that can increase the false-alarm rate was explored via a colored-loading framework. The method uses the observed response of strong scatterers to filter out these discrete scatterers prior to adaptive processing. Future work will attempt to quantify the improvement in false-alarm rate and sensitivity.

The proposed algorithms were tested using a homogeneous clutter simulation that represents a nominal X-band GMTI radar system as well as experimental data. Future work is required to determine the performance of the proposed techniques under other conditions and for varying system parameters such as larger scanning angles and higher bandwidths. The goal of the future work will be to develop a better theoretical understanding of the techniques via analysis and simulation and to determine under what operating conditions and for what types of systems they are best suited.

Finally, other approaches to multiresolution processing may prove fruitful. The concept of optimizing the radar resources (i.e., CPI length and bandwidth) to improve detection performance as a function of assumed target Doppler shift is an area that may lead to radar systems with significantly improved ability to track ground targets.

ACKNOWLEDGMENTS

The authors would like to acknowledge Dr. Paul Monticciolo and MIT Lincoln Laboratory for providing the Tuxedo data and Matlab programs that facilitated its analysis. The authors would like also to acknowledge Dr. Joseph Guerci of the DARPA Special Projects Office for discussions and insight regarding the development of the techniques described herein. This work was sponsored under Air Force Contract F30602-02-C-0005.

REFERENCES

[1] http://www.darpa.mil/spo/programs/kassper.htm.

[2] KASSPER '02: *A Premier Event*, Knowledge-Aided Sensor Signal Processing and Expert Reasoning Workshop Proceedings, Washington, DC, USA, April 2002.

[3] Knowledge-Aided Sensor Signal Processing and Expert Reasoning Workshop Conference Proceedings, Las Vegas, Nev, USA, April 2003.

[4] 3rd Annual (KASSPER '04) Workshop Conference Proceedings, Clearwater, Fla, USA, April 2004.

[5] J. S. Bergin, C. M. Teixeira, and P. M. Techau, "Multiresolution signal processing techniques for airborne radar," in *Proceedings of the 2003 KASSPER Workshop*, Las Vegas, NV, USA, April 2003.

[6] J. S. Bergin, C. M. Teixeira, and P. M. Techau, "Multiresolution signal processing techniques for airborne radar," in *Proc. 2004 IEEE Radar Conference*, Philadelphia, Pa, USA, April 2004.

[7] J. S. Bergin and P. M. Techau, "High fidelity site-specific radar simulation: KASSPER '02 workshop datacube," Tech. Rep. ISL-SCRD-TR-02-105, Information Systems Laboratories (ISL), Vienna, Va, USA, May 2002.

[8] J. S. Bergin and P. M. Techau, "High-fidelity site-specific radar simulation: KASSPER data set 2," Tech. Rep. ISL-SCRD-TR-02-106, Information Systems Laboratories (ISL), Vienna, Va, USA, October 2002.

[9] J. S. Bergin, P. M. Techau, W. L. Melvin, and J. R. Guerci, "GMTI STAP in target-rich environments: site-specific analysis," in *Proc. 2002 IEEE Radar Conference*, pp. 391–396, Long Beach, Calif, USA, April 2002.

[10] P. M. Techau, J. R. Guerci, T. H. Slocumb, and L. J. Griffiths, "Performance bounds for hot and cold clutter mitigation," *IEEE Transactions on Aerospace and Electronic Systems*, vol. 35, no. 4, pp. 1253–1265, 1999.

[11] J. B. Billingsley, "Exponential decay in windblown radar ground clutter Doppler spectra: multifrequency measurements and model," Tech. Rep. 997, MIT Lincoln Laboratory, Lexington, Mass, USA, July 1996.

[12] J. Ward, "Space-time adaptive processing for airborne radar," Tech. Rep. 1015, MIT Lincoln Laboratory, Lexington, Mass, USA, December 1994.

[13] J. R. Guerci, "Theory and application of covariance matrix tapers for robust adaptive beamforming," *IEEE Transactions on Signal Processing*, vol. 47, no. 4, pp. 997–985, 1999.

[14] P. M. Techau, J. S. Bergin, and J. R. Guerci, "Effects of internal clutter motion on STAP in a heterogeneous environment," in *Proceedings of 2001 IEEE Radar Conference*, pp. 204–209, Atlanta, Ga, USA, May 2001.

[15] R. C. DiPietro, "Extended factored space-time processing for airborne radar systems," in *Proceedings of 26th Annual Asilomar Conference on Signals, Systems, and Computing*, vol. 1, pp. 425–430, Pacific Grove, Calif, USA, October 1992.

[16] W. L. Melvin and J. R. Guerci, "Adaptive detection in dense target environments," in *Proceedings of 2001 IEEE Radar Conference*, pp. 187–192, Atlanta, Ga, USA, May 2001.

[17] A. Yegulalp, "FOPEN GMTI using multi-channel adaptive SAR," in *Proceedings of 10th Annual Adaptive Sensor Array Processing Workshop*, MIT Lincoln Laboratory, Lexington, Mass, USA, March 2002.

[18] M. I. Skolnik, *Radar Handbook*, McGraw-Hill, Boston, Mass, USA, 1990.

[19] J. S. Bergin, C. M. Teixeira, P. M. Techau, and J. R. Guerci, "Space-time beamforming with knowledge-aided constraints," in *Proceedings of Adaptive Sensor Array Processing Workshop*, MIT Lincoln Laboratory, Lexington, Mass, USA, March 2003.

[20] C. M. Teixeira, J. S. Bergin, and P. M. Techau, "Reduced degree-of-freedom STAP with knowledge-aided data prewhitening," in *Proceedings of 2003 KASSPER Workshop*, Las Vegas, Nev, USA, April 2003.

[21] J. S. Bergin, C. M. Teixeira, P. M. Techau, and J. R. Guerci, "Reduced degree-of-freedom STAP with knowledge-aided data pre-whitening," in *Proceedings of 2004 IEEE Radar Conference*, Philadelphia, Pa, USA, April 2004.

[22] J. S. Bergin, C. M. Teixeira, P. M. Techau, and J. R. Guerci, "STAP with knowledge-aided pre-whitening," in *Proceedings of the 2004 Tri-Service Radar Symposium*, pp. 289–294, Albuquerque, NM, USA, June 2004.

[23] W. L. Melvin, G. A. Showman, and D. J. Zywicki, "KA-STAP Development: GTRI Update," in *Briefing Presented at the KASSPER 2002 Program Review*, MIT Lincoln Laboratory, Lexington, Mass, USA, September 2002.

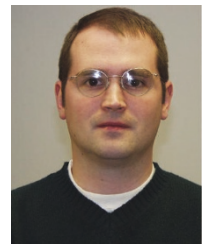

Jameson S. Bergin received his B.S.E.E. and M.S.E.E. degrees from the University of New Hampshire. He is a Principal Engineer with Information Systems Laboratories, Inc., in Vienna, Virginia. He has been with ISL since 1996. He has a background in digital signal processing, adaptive array processing, time series analysis, and communications systems. At ISL, he is modeling terrain-specific radar phenomenology including propagation, clutter, and hot clutter (terrain-scattered interference) and analyzing system performance. He has developed

simulation and analysis tools for STAP algorithm development and applied these tools to the analysis of both simulated and experimental data. At the University of New Hampshire, he was a Member of the Meteor Wind Radar Laboratory where his research included the use of higher-order spectral analysis techniques to detect nonlinear mixing of wind components in the upper atmosphere. In addition, he has analyzed problems such as radar system degradation due to Doppler quantization and nonuniform sampling.

Paul M. Techau received his M.S.E. degree from the University of Michigan and his B.S.E.E. degree from the University of Akron. He is a Vice President and Principal Engineer with Information Systems Laboratories, Inc., in Vienna, Virginia. He has been with ISL since 1988. Mr. Techau has a background in signal and array processing, detection and estimation theory, and radar and communications systems. For over ten years, he has led efforts to develop site-specific phenomenology models for radar and communications systems and is one of the first researchers to apply these models to system analyses including space-time adaptive processing (STAP) algorithm development. In addition, Mr. Techau has performed radar system research in areas including novel radar waveforms, tracking, and angle-of-arrival estimation. Mr. Techau is a Member of the IEEE, Tau Beta Pi, Eta Kappa Nu, and AFCEA.